Hindawi
Journal of Nanomaterials
Volume 2022, Article ID 2766317, 13 pages
https://doi.org/10.1155/2022/2766317

Research Article

Evaluating the Higher-Order Slip Consequence in Bioconvection Nanofluid Flow Configured by a Variable Thick Surface of Disk

Hassan Waqas,[1] **Sumeira Yasmin**,[1] **Nesreen Althobaiti**,[2] **Ebenezer Bonyah**,[3] **Ahmed Alshehri**,[4] **and Zahir Shah**[5]

[1]*Department of Mathematics, Government College University Faisalabad, Layyah Campus 31200, Pakistan*
[2]*Department of Mathematics and Statistics, College of Sciences, Taif University, P.O. Box 11099, Taif 21944, Saudi Arabia*
[3]*Department of Mathematics Education, University of Education Winneba Kumasi Campus, Kumasi 00233, Ghana*
[4]*Department of Mathematics, Faculty of Sciences, King Abdulaziz University, Jeddah 21589, Saudi Arabia*
[5]*Department of Mathematical Sciences, University of Lakki Marwat, Lakki Marwat, 28420 Khyber Pakhtunkhwa, Pakistan*

Correspondence should be addressed to Ebenezer Bonyah; ebbonya@gmail.com

Received 2 October 2021; Accepted 24 January 2022; Published 14 February 2022

Academic Editor: Amir Khan

For innovations in manufacturing and engineering scientific fields, the devices (electrical and computer systems) with large thermal effectiveness are needed. As a result, their thermal efficiency has become a very hot problem for many canvassers. With the novelty of this analysis, a mathematical study is performed to estimate the Darcy-Forchheimer flow of viscous magnetized fluid with Arrhenius activation energy and bioconvection effects through a variable thick surface of a rotating disk. The impact of thermal conductivity, heat source, and nonlinear thermal radiation is considered. The higher-order velocity slip impacts are also scrutinized. The system of partial differential equations (PDEs) and specific boundary restrictions is altered into a system of ODEs by adopting the suitable similarity transformations. The reduced ODE's system is tackled with the aid of shooting scheme under (bvp4c) built-in tool commercial software MATLAB. Moreover, the effects of different parameters over velocity components, thermal conductivity, concentration, and microorganism's fields are also examined. The confirmation of our findings is also explained through tables and graphical results. The results revealed that the radial velocity increases with the growing estimations of mixed convection parameter. The second-order velocity slip in radial direction causes a decrement in the estimation of axial velocity. Temperature distribution increases with a larger temperature ratio parameter. The concentration field of species and microorganism profile is reduced via a Brownian motion parameter and Peclet number, respectively.

1. Introduction

1.1. Literature Survey. Nanofluid is a fluid constructed with nanosized (1 to 100 nm) materials or molecules, named "nanomaterials" and otherwise "nanoparticles." Such substances are designed colloidal suspension of nanopowders in a continuous phase fluid. Nanoparticles utilized in nanofluids are constructed with oxidations, metals, and carbon nanotubes including carbides. Continuous phase fluids include ethanol glycol oil as well as water. Nanofluids have novel characteristics that build them potentially helpful in a broad range of heat transformation applications such as fuel cells, microprocessors, hybrid powered engines, pharmacological mechanisms, cooling equipment, chillers, refrigerators, and heat radiators in grinding, among others. Nanofluids are combinations of nanoparticles and the base fluids that can generate numerous heterogeneous nanofluids that are described for their thermophysical characteristics (thermal diffusivity and thermal conductivity, as well as viscosity) as a cooling system in heat transmission in comparison to base fluid, which increased with growing volumetric fraction of nanomaterials. Choi and Eastman [1] were firstly introduced to the basic idea of nanoparticles in constant phase fluids. Buongiorno [2] addressed nanoparticle study by developing a model to evaluate the thermal properties of continuous phase fluids. He predicted that the increased

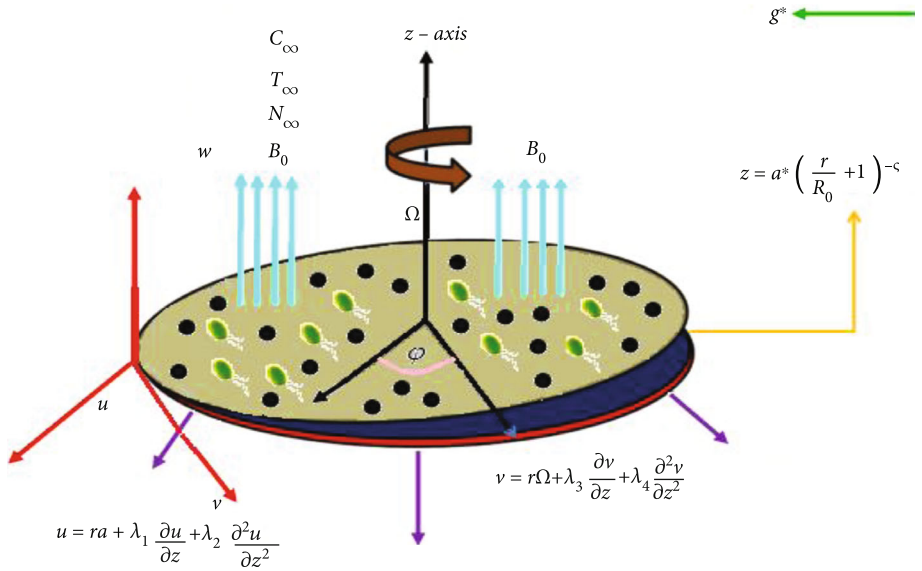

Figure 1: Schematic configuration of the flow problem.

conductance of constant phase fluid would be caused by the tiny-sized and lower volume fraction of supporting nanoelements. Nanotechnology is extremely important in numerous fields including chemical as well as metallurgical operating systems, transportation, macroscopic objects, cancer treatment, and electricity generation. Eid and Mabood [3] reported the suspending magnetohydrodynamic (MHD) flowing of micropolar dusty nanoparticles impinging on a permeability expanding sheet. Umar et al. [4] studied numerically the 3-dimensional incompressible Eyring-Powell nanofluid flow across a stretched surface including velocity slip as well as activation energy. Muhammad et al. [5] explored numerical simulations for 3-D Eyring–Powell (EP) nanoliquid under the nonlinear thermal radiation with changed heat and solutal fluxes. Rasool et al. [6] researched the Marangoni convective Casson-type flow of nanofluid impacted by the existence of Lorentz forces introduced into the modeling by an organized arrangement of magnets in the shape of the Riga configuration. Mahanthesh et al. [7] described the effect of quadratic thermal radiation as well as convection on the boundary layer 2-phase flowing of a dusty flow of nanoliquid through a vertical surface. Aaiza et al. [8] evaluate the magneto-nanoliquid flow across a channel in the presence of different nanoparticle shape factors. Hussanan et al. [9] investigate the thermal transportation phenomenon in micropolar water-based fluid. Khalid et al. [10] scrutinized the exact solution of nanofluid flow. Ali et al. [11] discussed the Brinkman-type nanofluid flow through vertical surface. Zin et al. [12] introduced the free convection behavior in Jeffery fluid through vertical porous surface.

The word activation energy plays a significant role in chemical reactions. The scientist Svante Arrhenius was the principal who initiated the description on activation energy in 1889 and that it is the minimum amount of energy required to initiate chemical reactions to a state in which they could experience material change. The application includes compound construction, food processing, transportation structures, a geothermal stored, and businesses. Heat and mass distribution aspects manage various mechanisms that were reacting synthetically which include the species composite reactions as well as codification strength having application in oil production and geothermal configuration. In actuality, it is the least amount of energy required to transform the reactants into substances. Activation energy can take the shape of kinetic and potential energy. It is essential to generate theoretical observations in addition to experimental contributions to measure the flow influence of activation energy. There have been very several theoretical efforts on this discussion. Indeed, the relationship between mass transfer and chemical reaction becomes tiresome. Such interactions can be observed both within the fluid and in mass transmission during the production process and employ of reactants at various levels. Bestman [13] clarified that viscoelastic fluid flow of thermal and mass moved in which restricts divider movements in its own plane utilizing a simplistic scientific theory of twofold material reaction with Arrhenius actuation energy. In this inspection, he obtained an analytical curriculum of action for the problem by employing an irritation method. Guo et al. [14] examined the kinetic model and thermodynamic of oxidant pyrolysis of microalgae wastes using a double distribution activation energy concept and simulating annealing. Hayat et al. [15] evaluated the effect of activation energy on entropy generation (EG) in a 3-dimensional magnetohydrodynamic (MHD) rotational flowing of nanofluids containing a binary chemical process. Araújo et al. [16] scrutinized the kinetic modeling and Arrhenius activation energy distributions in complicated systems with Hopfield Neural Network-based system. Elangovan and Natarajan [17] reported the primary treatment influences on qualitative characteristics, hydration diffusivity, and Arrhenius activation energy of solar drying gourd. The numerical analysis of unsteady Maxell nanofluid is simulated by Bilal et al. [18]. The effect of magneto nanofluid flow over disk with viscous dissipation is analyzed by Saeed et al. [19].

Table 1: Dimensionless prominent parameters.

Reynolds number	$\mathrm{Re} = \Omega R_0^2 \rho_f / \mu_f$
Mixed convection variable	$\lambda = \beta^{**} g * (1 - C_\infty)(T_f - T_\infty)/r\Omega^2$
Buoyancy ratio parameter	$\mathrm{Nr} = \left(\rho_p - \rho_f\right)(C_f - C_\infty)/\rho_f(1 - C_\infty)(T_f - T_\infty)\beta^{**}$
Bioconvection Rayleigh number	$\mathrm{Nc} = \gamma * \left(\rho_m - \rho_f\right)(N_f - N_\infty)/\rho_f(1 - C_\infty)(T_f - T_\infty)\beta^{**}$
Dimensionless constants	$\left(r^* = r/R_0^2, \varepsilon = r^*/(1 + r^*)\right)$
Magnetic parameter	$M = \sigma_f \beta_0^2 / \rho_f \Omega$
Local porosity parameter	$K_1^* = \nu_f / k^* \Omega$
Forchheimer number	$F_r = Fr,\ Fr = C_b^*/\sqrt{k^*}$
Eckert number	$\mathrm{Ec} = r^2\Omega^2/c_p(T_f - T_\infty)$
Brownian motion parameter	$\mathrm{Nb} = \tau D_B(C_f - C_\infty)/\nu_f$
Prandtl number	$\mathrm{Pr} = (\rho c_p \nu_f)/k_f$
Thermal source parameter	$Q\left(= Q^*/(\rho c_p)_f \Omega\right)$
Nonlinear thermal radiation parameter	$\mathrm{Rd} = 4\sigma^* T_\infty^3 / k^*$
Thermophoretic parameter	$\mathrm{Nt} = \tau D_T(T_f - T_\infty)/\nu_f T_\infty$
Activation energy parameter	$E_1 = E_a/\kappa T_\infty$
Schmidt number	$\mathrm{Sc} = \nu_f / D_B$
Stretching rate to angular frequency	$A_1 = a/\Omega$
First-order slip parameters in radial direction	$L_1 = (\lambda_1/R_0)(1 + r^*)^{\varsigma}\left(\Omega R_0^2 \rho_f/\mu_f\right)^{1/(n+1)} > 0,$ $L_3 = (\lambda_3/R_0)(1 + r^*)^{\varsigma}\left(\Omega R_0^2 \rho_f/\mu_f\right)^{1/(n+1)} > 0$
Tangential directional second-order slip parameters	$L_2 = \left(\lambda_2/R_0^2\right)(1 + r^*)^{2\varsigma}\left(\Omega R_0^2 \rho_f/\mu_f\right)^{2/(n+1)} < 0,$ $L_4 = \left(\lambda_4/R_0^2\right)(1 + r^*)^{2\varsigma}\left(\Omega R_0^2 \rho_f/\mu_f\right)^{2/(n+1)} < 0$
Thermal Biot number	$\Omega_1 = \left(h_1/k_f\right)(R_0/(1 + r^*)^{\varsigma})\left(\mu_f/\Omega R_0^2 \rho_f\right)^{1/(n+1)}$
Solutal Biot number	$\Omega_2 = (h_2/D_m)(R_0/(1 + r^*)^{\varsigma})\left(\mu_f/\Omega R_0^2 \rho_f\right)^{1/(n+1)}$
Microorganism Biot number	$\Omega_3 = (h_3/D_m)(R_0/(1 + r^*)^{\varsigma})\left(\mu_f/\Omega R_0^2 \rho_f\right)^{1/(n+1)}$
Chemical reaction parameter	$K_1 = k_r^2/\Omega$
Temperature ratio parameter	$\alpha_1 = (T_f - T_\infty)/T_\infty$
Disk thickness coefficient	$\alpha = \left(a/R_0^2\right)\left(\Omega R_0^2 \rho_f/\mu_f\right)^{-1/(n+1)}$
Bioconvective Lewis number	$\mathrm{Lb} = \nu/D_m$
Peclet number	$\mathrm{Pe} = bW_c/D_m$
Microorganism difference number	$\Omega_0 = N_\infty/N_f - N_\infty,$

Microorganism molecules have been widely used in the production of manufacturing and industrial products such as ethanol, waste-derived biofuel, and fertilizers. They are also utilized in water therapeutic facilities. These microorganisms generate hydrogen gas and biofuel, a favorable dispatchable energy source. As a result, we must investigate the swimming structures and mass transmission properties of microorganisms in order to make their applications more successful, profitable, and widespread for the benefit of humanity. Bioconvection is the production of various types of irregular fluid structures at the microscopic level therefore of the unexpected swimming of self-propelled microorganisms found in water or those certain denser fluids. Natural hypotheses such as searching for nutrients, oxygen for

breathing, and improving light absorption for photosynthesis influence the swimming of such microorganisms. Platt in 1961 [20] introduced the term "bioconvection" to illustrate the methodology of improvement of manners in depth suspensions of motile microorganisms at constant temperatures, in comparison to those reported under convectional conditions. Kuznetsov [21] proposed the concept of biothermal convection caused by temperature gradients as well as microorganism swimming. Tlili et al. [22] scrutinized the effect of bioconvection micropolar nanoliquid flow including gyrotactic motile microorganisms on thermal and solutal stratifications at the boundary layer. Al-Mubaddel et al. [23] examined Sisko-based nanofluid under the bioconvection radiation flow with specific thermal and solutal fluxes. Abbasi et al. [24] illustrated the flow of viscoelastic nanoparticles containing gyrotactic motile microorganisms across a rotating stretched disk under convective and zero mass flux conditions. Shehzad et al. [25] scrutinized the bioconvection of a Maxwell-based nanoliquid above an isolated rotational disk under the effect of double diffusional Cattaneo–Christov (C-C) concepts. Aziz et al. [26] evaluated the effects of motile microorganisms on unstable Williamson nanoliquid caused by a bidirectional accelerating surface. Alizadeh and Ganji [27] analyzed the two-phase thermosyphon utilizing RSM. The thermal transportation features and thermal resistance are discussed by Alizadeh and Ganji [28]. Some important research work about fluid flow and heat transfer can be studied in [29–31].

Taking the higher-order velocity slip consider, this communication extends the bioconvection nanofluid flow through a stretching disk. The Darcy-Forchheimer porous medium is considered. The heat transfer is incorporated in the presence of nonlinear thermal radiation, joule heating, thermophoresis, and Brownian diffusion. The significance of Arrhenius activation energy is considered. The dimensionless system is tackled by utilizing a shooting scheme with the bvp4c function of MATLAB. The effects of flow controlling parameters are analyzed.

2. Mathematical Description

2.1. Flow Analysis. Here, our main purpose is to scrutinize the steady three-dimensional, incompressible, and axially symmetric laminar flow of nanofluid including bioconvection with motile microorganism over a stretching disk surface. The schematic view of flow problem and the system of coordinates is depicted in Figure 1; here, the surface of the disk is stretchable through the rate of α and moving along own axis under an angular frequency Ω. Due to the stretchable and angular frequency as well as electrical conduction in the presence of electromagnetic field, the flow is produced. The suitable boundary conditions are applied at the disk surface. Here, no suction/injection is present at the disk surface, that is, $w = 0$. The velocity components denoted as $(u, v, \text{and } w)$ are along the $(r, \varphi, \text{and } z)$ axis, respectively. The temperature of fluid T_f, nanoparticle concentration of fluid C_f, bioconvection fluid N_f, ambient temperature T_∞, and ambient volumetric concentration C_∞ as well as ambient swimming organisms N_∞ are also presented at the surface of a stretching disk.

The governing partial deferential equations are expressed as [32, 33]

$$u_r + \frac{u}{r} + w_z = 0, \tag{1}$$

$$u\partial_r(u) - \frac{v^2}{r} + w_z(u) = \nu_f u_{zz} - \frac{\sigma_f \beta_0^2}{\rho_f} u - \frac{\nu_f}{k^*} u - Fu^2 + \frac{1}{\rho_f} \begin{bmatrix} (1-C_f)\rho_f \beta^{**} g * (T - T_\infty) \\ -\left(\rho_p - \rho_f\right) g^* (C - C_\infty) \\ -(N - N_\infty) g^* \gamma \left(\rho_m - \rho_f\right) \end{bmatrix}, \tag{2}$$

$$uv_r + \frac{uv}{r} + w_z(v) = \nu_f v_{zz} - \frac{\sigma_f \beta_0^2}{\rho_f} v - \frac{\nu_f}{k^*} v - Fv^2, \tag{3}$$

$$\begin{aligned} u_r(T) + w(T_z) = {} & \frac{1}{\rho c_p}[K(T_z)T_{zz}] + \frac{k_f}{(\rho c_p)_f} T_{zz} + \frac{\sigma_f \beta_0^2}{(\rho c_p)_f}\left(u^2 + v^2\right) \\ & + \frac{\mu_f}{(\rho c_p)_f}\left\{((u_z))^2 + (v_z)^2\right\} + \tau\left(D_B(T_z)\partial_z(C) + \frac{D_T}{T_\infty}(T_z)^2\right) \\ & + \frac{16\sigma^*}{3k^*(\rho c)_f}\left({T_z}^3 T_{zz}\right) + \frac{Q^*}{(\rho c_p)_f}(T - T_\infty), \end{aligned} \tag{4}$$

$$uC_r + wC_z = D_B[C_{zz}] + \frac{D_T}{T_\infty}[T_{zz}] - \mathrm{kr}^2(C - C_\infty)\left(\frac{T}{T_\infty}\right)^m \exp\left(\frac{-E_a}{\kappa T}\right), \tag{5}$$

$$uN_r + wN_z + [(N_z(C_{zz}))]\frac{bW_c}{(C_w - C_\infty)} = D_m(N_{zz}). \tag{6}$$

2.2. With Boundary Restrictions.

$$\begin{aligned} u &= ra + \lambda_1(u_z) + \lambda_2(u_{zz}), \\ v &= r\Omega + \lambda_3(v_z) + \lambda_4(v_{zz}), \\ w &= 0, \\ -k(T_z) &= h_1\left(T_f - T\right), \\ -D_B(C_z) &= h_2\left(C_f - C\right), \\ -D_m(N_z) &= h_3\left(N_f - N\right), \\ \text{at } z &= a^*\left(\frac{r}{R_0} + 1\right)^{-\varsigma}, \end{aligned} \tag{7}$$

$$\begin{aligned} u &\longrightarrow 0, \\ v &\longrightarrow 0, \\ T &\longrightarrow T_\infty, \\ C &\longrightarrow C_\infty, \\ N &\longrightarrow N_\infty, \end{aligned} \tag{8}$$

when $z \longrightarrow \infty$.

In the above governing equations, the velocity components are $u, v, \text{and } w$ along $r, \varphi, \text{and } z$ directions, ν_f represent the kinematic viscosity; σ_f is the electrical

conductivity of momentum; ρ_f is the fluid density of microorganism; K^* demonstrate the porous space permeability; β_0 is the magnetic field strength; $F(=C_b^*/r\sqrt{K^*})$ illustrate the coefficient of nonuniform inertia; g is the gravity; volume expansion coefficient is indicated by β^{**}; D_m represents the microorganism diffusion parameter; m exemplify the power law index; chemotaxis constant is expressed as b; the cell swimming speed is identified as W_e; C_b^* display the drag coefficient; T, C, and N are the basic temperature, volumetric concentration, and swimming bioconvection of fluid; k_f signify the thermal conductivity; c_p represents specific heat capacity; the heat capacitance ratio is symbolized by $\tau = (\rho c_p)_p/(\rho c_p)_f$; D_T represents thermophoresis diffusion coefficient; T_∞ stand for ambient temperature; m is the fitted rate constant; D_B represent the Brownian motion coefficient; the dynamic viscosity is μ_f, C_∞ and N_∞ are ambient concentration and ambient density microorganism, respectively; the rate of chemical reaction is k_r^2; $\beta_1, \beta_2, \beta_3$, and β_4 are linear/nonlinear thermal-based and nanoparticle concentration expansions; the exponential function is exp; the angular frequency is Ω; the activation energy is symbolized by E_a; the stretching constant is a; $\kappa = 8.61 \times 10^{-5}$ eV/K expressed the Stefan Boltzmann constant; $\lambda_1(\lambda_2 < 0)$ and $\lambda_3(\lambda_4 < 0)$ are the first- and second-order slip coefficients, respectively; and h_1 and h_2 are the heat mass transfer coefficient and the mass transfer coefficient, respectively.

2.3. Similarities. The similarity variables are

$$\begin{aligned} u &= r^* R_0 \Omega F(\eta), \\ v &= r^* R_0 \Omega G(\eta), \\ w &= R_0 \Omega (1+r^*)^{-\varsigma} \left(\frac{\Omega R_0^2 \rho_f}{\mu_f}\right)^{-1/(n+1)} H(\eta), \\ \Theta &= \frac{T - T_\infty}{T_f - T_\infty}, \\ \Phi &= \frac{C - C_\infty}{C_f - C_\infty}, \\ X &= \frac{N - N_\infty}{N_f - N_\infty}, \\ \eta &= \frac{z}{R_0}(1+r^*)^{\varsigma} \left(\frac{\Omega R_0^2 \rho_f}{\mu_f}\right)^{1/(n+1)}. \end{aligned} \tag{9}$$

In above transformations, radius is R_0; the power law index is n; the thickness power law index is ς; the components of velocity (radial, tangential, and axial) are symbolized by F, G, and H; and r^* is the constant of nondimensional radius. The temperature variable conductivity is addressed as

$$K(T) = k_\infty \left[1 + \epsilon_1 \left(\frac{T - T_\infty}{\Delta T}\right)\right]. \tag{10}$$

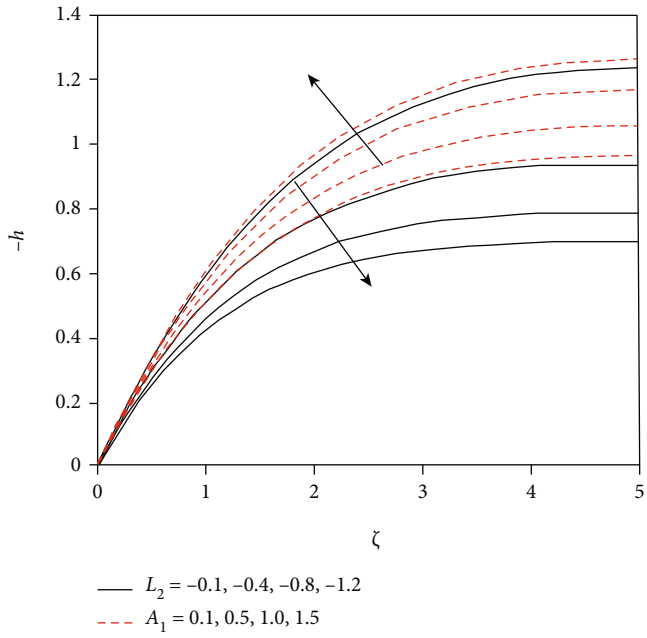

Figure 2: Fluctuation in axial velocity component against two different parameters.

2.4. Reduced Equations. The governing dimensionless equations after applying the suitable similarity transformation are expressed as

$$2F + H_\eta + \eta\varepsilon\varsigma F_\eta = 0, \tag{11}$$

$$\begin{aligned} &(\mathrm{Re})^{(1-n)/(1+n)}(1+r^*)^{2\varsigma} F_{\eta\eta} - 2F_\eta{}^2 + G^2 - HF - FF_\eta \varsigma\eta\varepsilon - MF \\ &\quad - K_1^* F - F_r F^2 + \lambda(\Theta - \mathrm{Nr}\Phi - \mathrm{Nc}X) = 0, \end{aligned} \tag{12}$$

$$(\mathrm{Re})^{(1-n)/(1+n)}(1+r^*)^{2\varsigma} G_{\eta\eta} - 2FG - HG_\eta - FG_\eta \varsigma\eta\varepsilon - MG - K_1^* G - F_r G^2 = 0, \tag{13}$$

$$\begin{aligned} &\frac{1}{pr}(\mathrm{Re})^{(1-n)/(1+n)}(1+r^*)^{2\varsigma}(1+\epsilon_1)\Theta_{\eta\eta} + \epsilon_1 \Theta_\eta{}^2 \\ &\quad + \frac{4}{3}\mathrm{Rd}\begin{bmatrix} \Theta_{\eta\eta} + (\theta_w - 1)^3\left(3\Theta^2\Theta_\eta{}^2 + \Theta^3\Theta_{\eta\eta}\right) \\ +3(\Theta_w - 1)^2\left(2\Theta\Theta_\eta{}^2 + \Theta^2\Theta_{\eta\eta}\right) \\ +3(\Theta_w - 1)\left(\Theta_\eta{}^2 + \Theta\Theta_{\eta\eta}\right) \end{bmatrix} - H\Theta_\eta \\ &\quad - F\Theta_\eta \varsigma\eta\varepsilon + \mathrm{Nt}(\mathrm{Re})^{(1-n)/(1+n)}(1+r^*)^{2\varsigma}\Theta_\eta{}^2 \\ &\quad + \mathrm{Nb}(\mathrm{Re})^{(1-n)/(1+n)}\Theta_\eta\Phi_\eta + M\mathrm{Ec}\left(F^2 + G^2\right) \\ &\quad + \mathrm{Ec}(\mathrm{Re})^{(1-n)/(1+n)}(1+r^*)^{\varsigma}\left(F_\eta{}^2 + G_\eta{}^2\right) + Q\Theta = 0, \end{aligned} \tag{14}$$

$$\begin{aligned} &\left(\frac{\mathrm{Nt}}{\mathrm{Nb}}\right)(\mathrm{Re})^{(1-n)/(1+n)}(1+r^*)^{2\varsigma}\Theta_{\eta\eta} + (\mathrm{Re})^{(1-n)/(1+n)}(1+r^*)^{2\varsigma}\Phi_{\eta\eta} \\ &\quad - \mathrm{Sc}\varsigma\eta\varepsilon F\Theta_\eta - \mathrm{Sc}H\Phi_\eta - K_1\Phi(1+\alpha_1\Theta)^m \exp\left[\frac{-E_1}{(1+\alpha_1\Theta)}\right] = 0, \end{aligned} \tag{15}$$

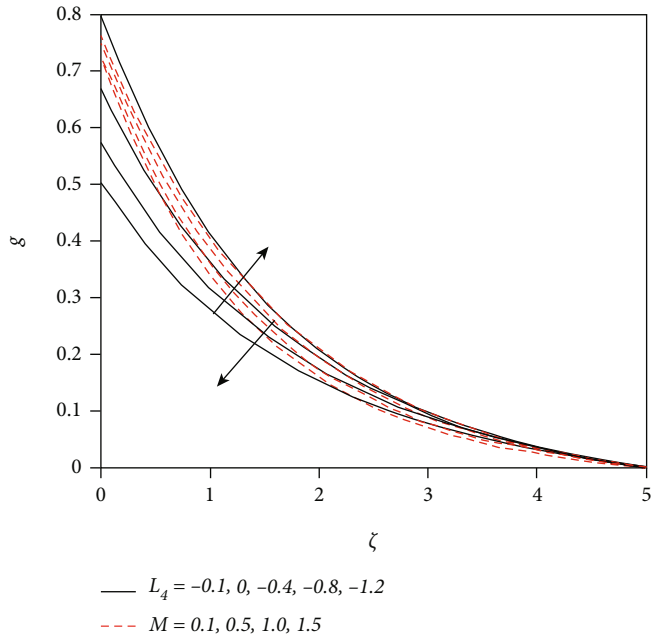

Figure 3: Fluctuation in tangential velocity component against two different parameters.

$$(\mathrm{Re})^{(1-n)/(1+n)}(1+r^*)^{2\varsigma}X_{\zeta\zeta} - \mathrm{Lb}HX_\zeta + \mathrm{Lb}\varsigma\eta\varepsilon FX_\eta - \mathrm{Pe}\left(\Phi_{\eta\eta}(X+\Omega_0) + X_\eta\Phi_\eta\right) = 0, \tag{16}$$

with

$$\begin{aligned} F(\alpha) &= A + L_1F_\eta(\alpha) + L_2F_{\eta\eta}(\alpha),\\ G(\alpha) &= 1 + L_3G_\eta(\alpha) + L_4G_{\eta\eta}(\alpha),\\ H(\alpha) &= 0,\\ \Theta_\eta(\alpha) &= -\Omega_1(1-\Theta(\alpha)),\\ \Phi_\eta(\alpha) &= -\Omega_2(1-\Phi(\alpha)),\\ X_\eta(\alpha) &= -\Omega_3(1-X(\alpha)), \end{aligned} \tag{17}$$

$$\begin{aligned} F(\infty) &\longrightarrow 0,\\ G(\infty) &\longrightarrow 0,\\ \Theta(\infty) &\longrightarrow 0,\\ \Phi(\infty) &\longrightarrow 0,\\ X(\infty) &\longrightarrow 0. \end{aligned} \tag{18}$$

The following are currently considered for introducing the innovative similarity transformation to modify the origin from α to 0, that is,

$$\begin{aligned} H(\eta) &= h(\eta-\alpha) = h(\zeta),\\ F(\eta) &= f(\eta-\alpha) = f(\zeta),\\ G(\eta) &= g(\eta-\alpha) = g(\zeta),\\ \Theta(\eta) &= \theta(\eta-\alpha) = \theta(\zeta),\\ \Phi(\eta) &= \phi(\eta-\alpha) = \phi(\zeta),\\ X(\eta) &= \chi(\eta-\alpha) = \chi(\zeta). \end{aligned} \tag{19}$$

We get

$$2f + h_\zeta + (\zeta+\alpha)\varsigma\varepsilon F_\zeta = 0, \tag{20}$$

$$\begin{aligned} &(\mathrm{Re})^{(1-n)/(1+n)}(1+r^*)^{2\varsigma}f_{\zeta\zeta} - 2f_\zeta{}^2 + g^2 - hf - ff_\zeta\varsigma(\eta+\alpha)\varepsilon - Mf - K_1^*f - F_rf^2\\ &\quad + \lambda(\theta - \mathrm{Nr}\phi - \mathrm{Nc}\chi) = 0, \end{aligned} \tag{21}$$

$$(\mathrm{Re})^{(1-n)/(1+n)}(1+r^*)^{2\varsigma}g_{\zeta\zeta} - 2fg - hg_\zeta - fg_\zeta\varsigma(\eta+\alpha)\varepsilon - Mg - K_1^*g - F_rg^2 = 0, \tag{22}$$

$$\begin{aligned} &\frac{1}{pr}(\mathrm{Re})^{(1-n)/(1+n)}(1+r^*)^{2\varsigma}(1+\epsilon_1)\theta_{\zeta\zeta} + \epsilon_1\theta_\zeta{}^2 + \frac{4}{3}\mathrm{Rd}\begin{bmatrix}\theta_{\zeta\zeta} + (\theta_w-1)^3\left(3\theta^2\theta_\zeta{}^2 + \theta^3\theta_{\zeta\zeta}\right)\\ +3(\theta_w-1)^2\left(2\theta\theta_\zeta{}^2 + \theta^2\theta_{\zeta\zeta}\right)\\ +3(\theta_w-1)\left(\theta_\zeta{}^2 + \theta\theta_{\zeta\zeta}\right)\end{bmatrix}\\ &\quad - h\theta_\zeta - f\theta_\zeta\varsigma(\zeta+\alpha)\varepsilon + \mathrm{Nt}(\mathrm{Re})^{(1-n)/(1+n)}(1+r^*)^{2\varsigma}\theta_\zeta{}^2 + \mathrm{Nb}(\mathrm{Re})^{(1-n)/(1+n)}\theta_\zeta\phi_\zeta\\ &\quad + M\mathrm{Ec}\left(f^2+g^2\right) + \mathrm{Ec}(\mathrm{Re})^{(1-n)/(1+n)}(1+r^*)^\varsigma\left(f_\zeta{}^2 + g_\zeta{}^2\right) + Q\theta = 0, \end{aligned} \tag{23}$$

$$\left(\frac{\mathrm{Nt}}{\mathrm{Nb}}\right)(\mathrm{Re})^{(1-n)/(1+n)}(1+r^*)^{2\varsigma}\theta_{\zeta\zeta}+(\mathrm{Re})^{(1-n)/(1+n)}(1+r^*)^{2\varsigma}\phi_{\zeta\zeta}-\mathrm{Sc}\varsigma(\zeta+\alpha)\varepsilon f\theta_\zeta - \mathrm{Sc}h\phi_\zeta - K_1\phi(1+\alpha_1\theta)^m\exp\left[\frac{-E_1}{(1+\alpha_1\theta)}\right]=0, \tag{24}$$

$$(\mathrm{Re})^{(1-n)/(1+n)}(1+r^*)^{2\varsigma}\chi_{\zeta\zeta}-\mathrm{Lb}h\chi_\zeta+\mathrm{Lb}\varsigma(\zeta+\alpha)\varepsilon f\chi_\zeta-\mathrm{Pe}\left(\phi_{\zeta\zeta}(\chi+\Omega)+\chi_\zeta\phi_\zeta\right)=0, \tag{25}$$

through boundary conditions

$$\begin{aligned} f(0)&=A_1+L_1f_\zeta(0)+L_2f_{\zeta\zeta}(0),\\ g(0)&=1+L_3g_\zeta(0)+L_4g_{\zeta\zeta}(0),\\ h(0)&=0,\\ \theta_\zeta(0)&=-\Omega_1(1-\theta(0)),\\ \phi_\zeta(0)&=-\Omega_2(1-\phi(0)),\\ \chi_\zeta(0)&=-\Omega_3(1-\chi(0)), \end{aligned} \tag{26}$$

$$\begin{aligned} f(\infty)&\longrightarrow 0,\\ g(\infty)&\longrightarrow 0,\\ \theta(\infty)&\longrightarrow 0,\\ \phi(\infty)&\longrightarrow 0,\\ \chi(\infty)&\longrightarrow 0. \end{aligned} \tag{27}$$

2.5. Dimensionless Prominent Parameters. Now, the dimensionless prominent parameters are given in Table 1.

2.6. Physical Quantities. Here, the local skin friction coefficient (LSF) C_f, local Nusselt number (LNN) Nu_x, local Sherwood number (LSW) Sh_x, and density motile microorganism (LMN) Sn_x are represented as follows:

Local skin friction coefficient

$$C_f=\frac{\sqrt{\tau_{zr}^2+\tau_{z\theta}^2}}{\rho_f(\Omega r)^2}. \tag{28}$$

Here, τ_{zr} and $\tau_{z\theta}$ are expressed as

$$\tau_{zr}=\mu_f(u_z)\Big|_{z=0}=\mu_f r^*\Omega_1(1+r^*)^\varsigma\left(\frac{\Omega R_0^2\rho_f}{\mu_f}\right)^{1/(n+1)}f_\zeta(0), \tag{29}$$

$$\tau_{z\theta}=\mu_f(v_z)\Big|_{z=0}=\mu_f r^*\Omega_1(1+r^*)^\varsigma\left(\frac{\Omega R_0^2\rho_f}{\mu_f}\right)^{1/n+1}g_\zeta(0). \tag{30}$$

Here, τ_w is identified as

$$\tau_w=\sqrt{\tau_{zr}^2+\tau_{z\theta}^2}. \tag{31}$$

Finally, local skin friction coefficient

$$C_{fx}\,\mathrm{Re}^{(n-1)/(n+1)}=\frac{\tau_w|_{z=0}}{\rho_f(r\Omega)^2}=\frac{1}{r^*}(1+r^*)^\varsigma\left[\left(f_\zeta(0)\right)^2+\left(g_\zeta(0)\right)^2\right]^{1/2}. \tag{32}$$

Here, τ_{zr} denoted the shear stress along the radial direction, $\tau_{z\theta}$ represent the shear stress along the direction of tangential, and τ_w denoted the shear stress.

Local Nusselt number

$$\mathrm{Nu}_x=\frac{R_0q_w}{k_f\left(T_f-T_\infty\right)}\Bigg|_{z=0}. \tag{33}$$

Here, q_w is symbolized as

$$q_w|_{z=0}=-k_f(T_z)\big|_{z=0}=-k_f\left(T_f-T_\infty\right)(1+r^*)^\varsigma\left(\frac{\Omega R_0^2\rho_f}{\mu_f}\right)^{1/(n+1)}\theta_\zeta(0). \tag{34}$$

Finally, the local Nusselt number

$$\mathrm{Re}^{-1/(n+1)}\mathrm{Nu}_x=-(1+r^*)^\varsigma\theta_\zeta(0). \tag{35}$$

Local Sherwood number

$$\mathrm{Sh}_x=\frac{R_0q_m}{D_B\left(C_f-C_\infty\right)}\Bigg|_{z=0}. \tag{36}$$

Here, q_m is denoted as

$$q_m=-D_B(C_z)|_{z=0}. \tag{37}$$

Finally, the local Sherwood number

$$\mathrm{Sh}_x\,\mathrm{Re}^{-1/(n+1)}=-(1+r^*)^\varsigma\phi_\zeta(0). \tag{38}$$

Density motile microorganism number

$$\mathrm{Sn}_x=\frac{R_0q_n}{D_m\left(N_f-N_\infty\right)}\Bigg|_{z=0}. \tag{39}$$

Here, q_n is identified as

$$q_n=-D_m(N_z)|_{z=0}. \tag{40}$$

Finally, the density motile microorganism number

$$\mathrm{Sn}_x\,\mathrm{Re}^{-1/(n+1)}=-(1+r^*)^\varsigma\chi_\zeta(0). \tag{41}$$

3. Numerical Scheme

Significantly, the method of finding the exact solution for momentum, temperature, nanoparticle concentration, and bioconvection equations through corresponding initial

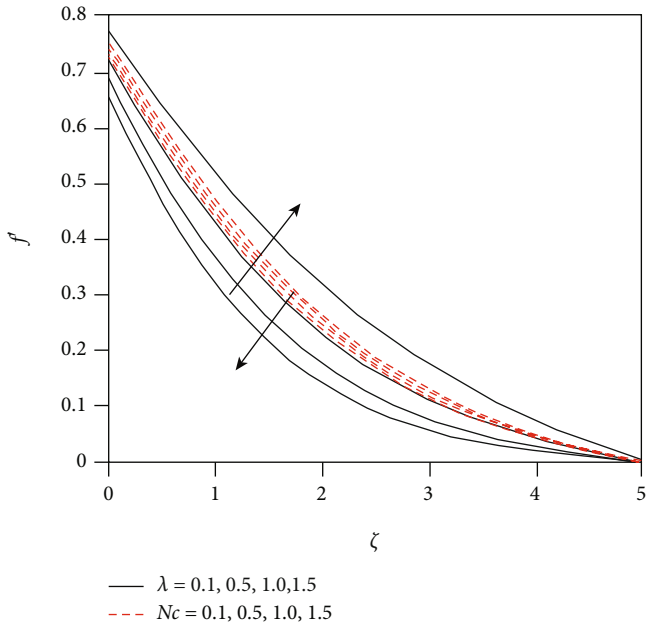

Figure 4: Fluctuation in radial velocity component against two different parameters.

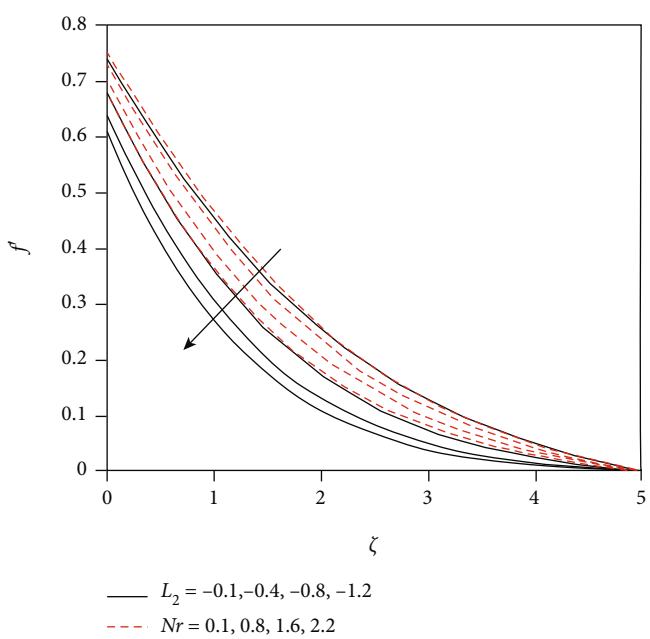

Figure 5: Fluctuation in radial velocity component against two different parameters.

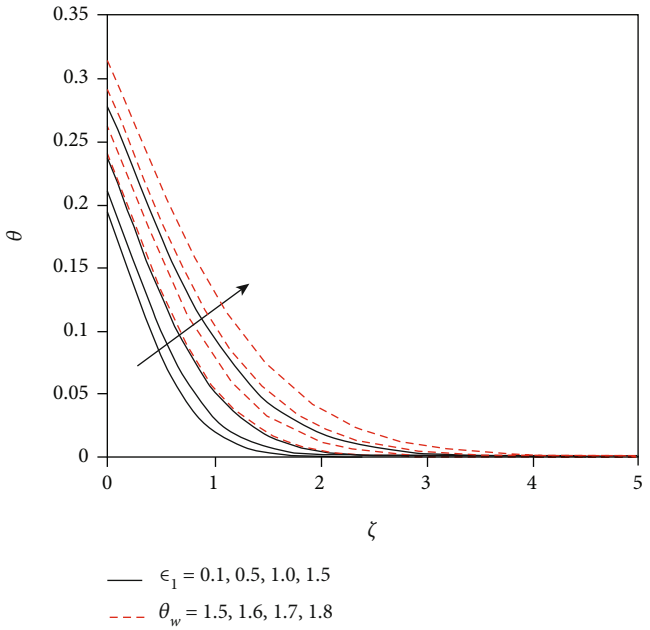

Figure 6: Fluctuation in thermal field against two different parameters.

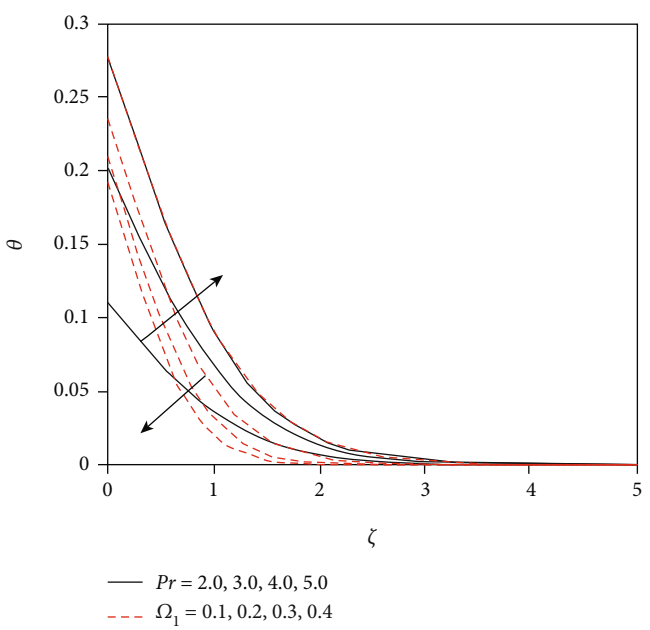

Figure 7: Fluctuation in thermal field against two different parameters.

conditions is very complicated and doubtful about the significance of results. Researchers have attempted to mathematically research the nanoliquid flowing past the stretching disk. Chemical processes, including activation energy, are also used to research the characteristics of mass transformation. Choose the initial guesses, and the dimensionless highly linear governing equations ((20))–((25)) with the related boundary conditions ((26))-((27)) are numerically integrated by utilizing the computational software MATLAB through built-in rule bvp4c (shooting method). The bvp4c method is a powerful way of resolving an initial value problem and a well-known methodology to find more than one solution. In order to solve these equations, first, we converted the higher-order differential equation into a first-order system by using the following technique.

We identify new variables as

$$\begin{aligned} h &= r_1, \\ h_\zeta &= r_1', \\ f &= r_2, \\ f_\zeta &= r_3, \\ f_{\zeta\zeta} &= r_3', \\ g &= r_4, \\ g_\zeta &= r_5, \\ g_{\zeta\zeta} &= r_5', \\ \theta &= r_6, \\ \theta_\zeta &= r_7, \\ \theta_{\zeta\zeta} &= r_7', \\ \phi &= r_8, \\ \phi_\zeta &= r_9, \\ \phi_{\zeta\zeta} &= r_9', \\ \chi &= r_{10}, \\ \chi_\zeta &= r_{11}, \\ \chi_{\zeta\zeta} &= r_{11}', \end{aligned} \tag{42}$$

$$r_1' = -2r_2 - (\zeta + \alpha)\varsigma\varepsilon r_3, \tag{43}$$

$$r_3' = \frac{2r_3^2 - r_4^2 + r_1 r_2 + r_2 r_3 \varsigma(\zeta + \alpha)\varepsilon + Mr_2 + K_1^* r_2 + F_r r_2^2 - \lambda(r_6 - \mathrm{Nr} r_8 - \mathrm{Nc} r_{10})}{(\mathrm{Re})^{(1-n)/(1+n)}(1 + r^*)^{2\varsigma}}, \tag{44}$$

$$r_5' = \frac{2r_2 r_4 + r_1 r_5 + r_2 r_5 \varsigma(\zeta + \alpha)\varepsilon + Mr_4 + K_1^* r_4 + F_r r_4^2}{(\mathrm{Re})^{(1-n)/(1+n)}(1 + r^*)^{2\varsigma}}, \tag{45}$$

$$r_7' = \frac{r_1 r_7 - \epsilon_1 r_7^2 + r_2 r_7 \varsigma(\zeta + \alpha)\varepsilon - \mathrm{Nt}(\mathrm{Re})^{(1-n)/(1+n)}(1 + r^*)^{2\varsigma} r_7^2 - \mathrm{Nb}(\mathrm{Re})^{(1-n)/(1+n)} r_7 r_9 - M\mathrm{Ec}(r_2^2 + r_4^2) - \mathrm{Ec}(\mathrm{Re})^{(1-n)/(1+n)}(1 + r^*)^{\varsigma}(r_3^2 + r_5^2) - (4/3)\mathrm{Rd}\left[(\theta_w - 1)^3(3r_6^2 r_7^2) + 3(\theta_w - 1)^2(2r_6 r_{7\zeta}^2) + 3(\theta_w - 1)(r_7^2)\right] - Qr_6}{(1)/pr(\mathrm{Re})^{(1-n)/(1+n)}(1 + r^*)^{2\varsigma}(1 + \epsilon_1) + (4/3)\mathrm{Rd}(1 + (\theta_w - 1)^3 r_6^3 + 3(\theta_w - 1)^2 r_6^2 + 3(\theta_w - 1)r_6)}, \tag{46}$$

$$r_9' = \frac{-(\mathrm{Nt}/\mathrm{Nb})(\mathrm{Re})^{(1-n)/(1+n)}(1 + r^*)^{2\varsigma} r_7' + \mathrm{Sc}\varsigma(\zeta + \alpha)\varepsilon r_2 r_7 + \mathrm{Scr}_1 r_9 + K_1 r_8(1 + \alpha_1 r_6)^m \exp\left[-E_1/(1 + \alpha_1 r_6)\right]}{(\mathrm{Re})^{(1-n)/(1+n)}(1 + r^*)^{2\varsigma}}, \tag{47}$$

$$r_{11}' = \frac{\mathrm{Lbr}_1 r_{11} - \mathrm{Lb}\varsigma(\zeta + \alpha)\varepsilon r_2 r_{11} + \mathrm{Pe}\left(r_9'(r_{10} + \Omega) + r_{11} r_9\right)}{(\mathrm{Re})^{(1-n)/(1+n)}(1 + r^*)^{2\varsigma}}, \tag{48}$$

$$r_2(0) = A_1 + L_1 r_3(0) + L_2 r_3'(0), r_4(0) = 1 + L_3 r_5(0) + L_4 r_5'(0), r_1(0) = 0, r_7(0) = -\Omega_1(1 - r_6(0)), r_9(0) = -\Omega_2(1 - r_8(0)), r_{11}(0) = -\Omega_3(1 - r_{10}(0)), \tag{49}$$

$$r_2(\infty) \longrightarrow 0, r_4(\infty) \longrightarrow 0, r_6(\infty) \longrightarrow 0, r_8(\infty) \longrightarrow 0, r_{10}(\infty) \longrightarrow 0. \tag{50}$$

4. Result and Discussion

The aim of this portion is to envisage variations in velocity components, thermal field, concentration of nanoparticles, and microorganism profile due to interesting involved parameters introduced during the flow of bioconvective nanofluid that are demonstrated in Figures 2–10. Figure 2 explains the effects of second-order slip parameter and stretching rate to angular frequency. The escalating estimations of stretching rate to frequency exaggerate the axial velocity component. From this scenario, it can be detected that axial velocity of nanofluid decays via larger variations in second-order velocity slip parameter. Figure 3 communicates the impacts of second-order velocity slip as well as magnetic parameter versus tangential velocity. It can be observed that tangential velocity boosts up via larger second-order velocity slip parameter. Here, we also observe that the larger estimations in magnetic parameter diminishes

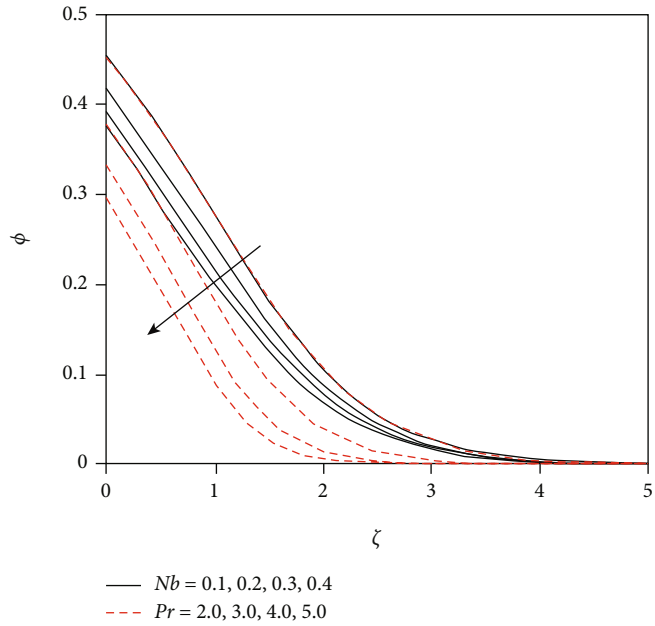

Figure 8: Fluctuation in concentration field against two different parameters.

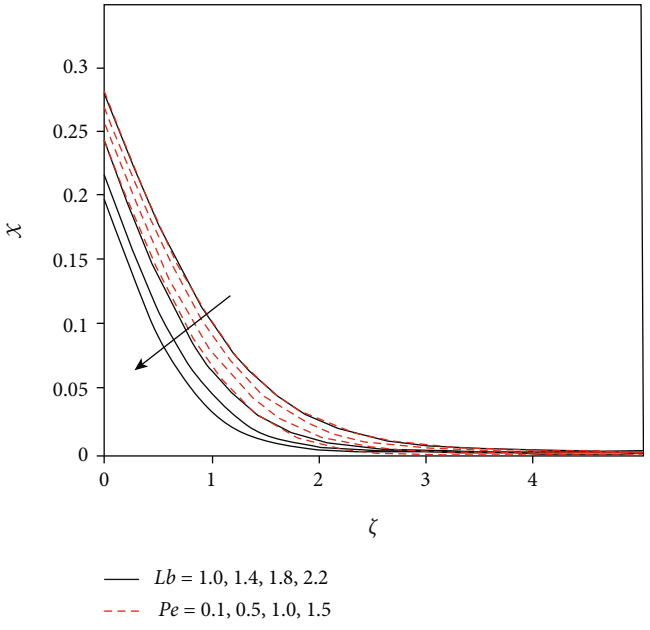

Figure 9: Fluctuation in the microorganism's field against two different parameters.

the tangential velocity of nanofluid flow. In terms of physics, the magnetic parameter is associated to the Lorentz force, which is a resistive force to the fluid flow. As the magnetic parameter increases, the resistance forces increase, and the velocity decreases. Figure 4 demonstrates the features of mixed convection parameter as well as bioconvection Rayleigh number over a radial velocity component. It is noticed that velocity is improved by growing the estimations of mixed convection parameter while it depresses via a greater bioconvection Rayleigh number. The features of buoyancy ratio parameter and second-order velocity slip parameter versus radial component of velocity are elaborated through Figure 5. The radial velocity is a decreasing function of second-order velocity slip parameter and buoyancy ratio parameter. Physically, for a given buoyancy impact, bioconvection inhibits the up movement of solid particles that arise in nanofluid; however, for a higher buoyancy impact, the fluid resists the fluid, resulting in fluid movement decline.

Figure 6 examines the behavior of thermal conductivity and temperature ratio parameter via thermal distribution of nanomaterials. It is witnessed that temperature field upsurges due to an increment in thermal conductivity and temperature ratio parameter. Figure 7 portrays the impression of Prandtl number and thermal Biot number versus temperature field. It is mentioned that improving Prandtl number reduces the temperature distribution. From this communication, we analyzed that enhancing the thermal Biot number escalates thermal field. Physically, when the Prandtl number rises, the thermal diffusivity diminishes. Fluid temperature drops as a result of the lower thermal diffusivity. Figure 8 presents the trend of the Brownian motion coefficient and Prandtl number against solutal field. Here, concentration reduces via a greater amount of Brownian motion coefficient as well as Prandtl number. Micromixing and heat conduction in the nanofluid are aided by enhancing the Brownian motion parameter, causing the temperature to rise and the nanoparticles to scatter more widely.

Figure 9 shows the nature of bioconvection Lewis number and Peclet number over a microorganism's field. It is concluded that the microorganism field diminishes by increasing the variations of bioconvection Lewis number and Peclet number. The bioconvection Lewis number has an converse relationship with microorganism diffusivity. As the bioconvection Lewis number rises, the diffusivity decreases, and the microorganism profile drops. The features

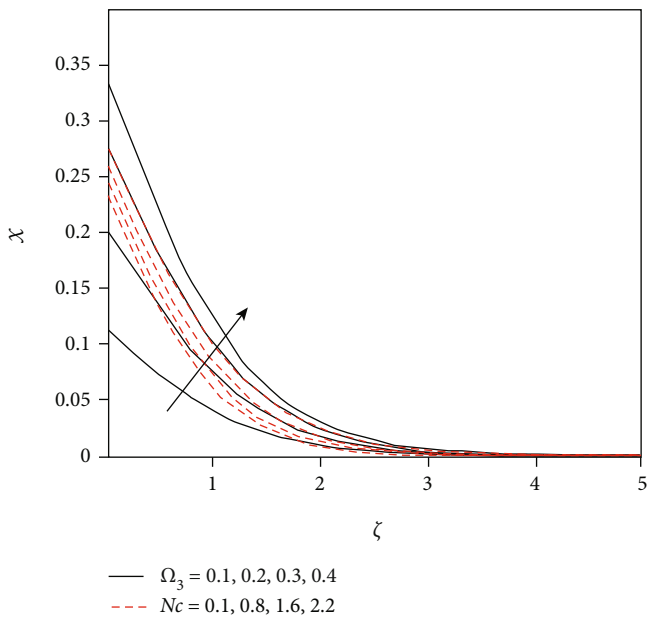

Figure 10: Fluctuation in the microorganism's field against two different parameters.

Table 2: Validation in results between published literature and current outcomes are present.

	$f''(0)$	$g'(0)$	$\theta'(0)$
Xun et al. [29]	0.51023	0.61592	0.39627
Anderson et al. [30]	0.510	0.616	0.3963
Ming et al. [31]	0.51021	0.61591	0.39632
Khan et al. [33]	0.51082	0.61595	0.3958
Current results	0.51084	0.61598	0.3958

of microorganism Biot number and bioconvection Rayleigh number are mentioned in Figure 10. It is noted that larger magnitudes of microorganism Biot number and bioconvection Rayleigh number increases the microorganism's profile. Here, it was analyzed that good validation in results between published literature and current outcomes is presented in Table 2.

5. Conclusion

Computational analysis is conducted on bioconvective viscous nanofluid flow past a stretching disk with higher-order slips and nonlinear thermal radiation. The main outcomes are listed as follows:

(i) Axial velocity component escalates versus a larger amount of stretching rate to angular frequency

(ii) Tangential velocity is increases against a second-order slip parameter

(iii) The increment in radial velocity has been analyzed along with increments in mixed convection parameter

(iv) The larger slip parameter and buoyancy ratio parameter reduce the radial velocity of nanofluid

(v) Thermal field of species rises against temperature-dependent thermal conductivity

(vi) Temperature distribution is increased via the temperature ratio parameter

(vii) Greater values of the thermal Biot number boost the temperature field

(viii) Concentration is reduced against the Brownian motion parameter

(ix) The microorganism's profile boosts via the microorganism's Biot number while it diminishes against the Peclet number

(x) The microorganism's field is depressed against the bioconvection Lewis number

Nomenclature

(u, v, w): Velocity components $(\mathrm{m \cdot s^{-1}})$
(r, φ, z): Coordinates of system (m)
ν_f: Kinematic viscosity
F: Inertia coefficient
k^*: Porous permeability
b: Chemotaxis constant
σ_f: Electrical conductivity
g^*: Gravitational acceleration
β^{**}: Volume expansion coefficient
D_T: Thermophoretic diffusion coefficient
D_m: Microorganism coefficient
τ: Capacity ratio
σ^*: Stefan Boltzmann number
kr^2: Chemical reaction coefficient
E_a: Coefficient of activation energy
N_∞: Ambient microorganisms
W_c: Cell swimming speed
N_f: Surface microorganisms
K_1^*: Chemical reaction parameter
K_1: Chemical reaction parameter
F_r: Darcy Forchheimer parameter
λ: Mixed convection parameter
M: Magnetic parameter
Nr: Buoyancy ratio parameter
Nc: Bioconvection Rayleigh number
Lb: Bioconvection Lewis number
α_1: Temperature ratio parameter
τ_{zr}: Radial directional shear stress
$\tau_{z\theta}$: Tangential directional shear stress
Pe: Peclet number
Ω_0: Microorganism difference parameter
A: Stretching ratio to angular frequency
L_1: Radial direction first-order velocity slip
Sh_x: LSN
Sn_x: LMN
ρ_f: Fluid density $(\mathrm{kg/m^3})$

ρ_p: Nanoparticle density
ρ_m: Microorganism density
k_f: Thermal conductivity ($Wm^{-1}K^{-1}$)
c_p: Specific heat (J/K)
$(\rho c_p)_f$: Heat capacity ($Jm^{-3}K^{-1}$)
T_∞: Ambient temperature
β_0: Magnetic field strength ($N{\cdot}m^{-1}{\cdot}A^{-1}$)
D_B: Brownian diffusion coefficient
k^*: Mean absorption coefficient
λ_3, λ_4: Coefficient of velocity slips
h_1, h_2, h_3: Heat, mass, microorganism transfer coefficient
Nb: Brownian motion parameter
C_∞: Ambient concentration
T_f: Surface temperature
C_f: Surface concentration
Re: Reynolds number
Pr: Prandtl number
Rd: Thermal radiation parameter
θ_w: Temperature difference parameter
E_1: Activation energy parameter
Nt: Thermophoresis parameter
Ec: Eckert number
Sc: Schmidt number
L_2: Radial direction second-order velocity slip
L_3: Tangential direction first-order velocity slip
L_4: Tangential direction second-order velocity slip
Ω_1: Thermal Biot number
Ω_2: Mass Biot number
Ω_3: Microorganism Biot number
C_f: Skin friction coefficient
Nu_x: LNN
Nu_x: Nusselt number
τ_w: Shear stress

Data Availability

The data that support the findings of this study are available from the corresponding author upon reasonable request.

Conflicts of Interest

The authors proclaim that they have no competing interests.

References

[1] S. U. S. Choi and J. A. Eastman, "Enhancing thermal conductivity of fluids with nanoparticles," in *1995 International mechanical engineering congress and exhibition*, United States, 1995.

[2] J. Buongiorno, "Convective transport in nanofluids," *Journal of Heat Transfer*, vol. 128, pp. 240–250, 2006.

[3] M. R. Eid and F. Mabood, "Entropy analysis of a hydromagnetic micropolar dusty carbon NTs-kerosene nanofluid with heat generation: Darcy–Forchheimer scheme," *Journal of Thermal Analysis and Calorimetry*, vol. 143, no. 3, pp. 2419–2436, 2021.

[4] M. Umar, R. Akhtar, Z. Sabir et al., "Numerical treatment for the three-dimensional Eyring-Powell fluid flow over a stretching sheet with velocity slip and activation energy," *Advances in Mathematical Physics*, vol. 2019, 2019.

[5] T. Muhammad, H. Waqas, S. A. Khan, R. Ellahi, and S. M. Sait, "Significance of nonlinear thermal radiation in 3D Eyring–Powell nanofluid flow with Arrhenius activation energy," *Journal of Thermal Analysis and Calorimetry*, vol. 143, no. 2, pp. 929–944, 2021.

[6] G. Rasool, A. Shafiq, and C. M. Khalique, "Marangoni forced convective Casson type nanofluid flow in the presence of Lorentz force generated by Riga plate," *Discrete & Continuous Dynamical Systems-S.*, vol. 14, no. 7, pp. 2517–2533, 2021.

[7] B. Mahanthesh, J. Mackolil, M. Radhika, and W. Al-Kouz, "Significance of quadratic thermal radiation and quadratic convection on boundary layer two-phase flow of a dusty nanoliquid past a vertical plate," *International Communications in Heat and Mass Transfer*, vol. 120, article 105029, 2021.

[8] G. Aaiza, I. Khan, and S. Shafie, "Energy transfer in mixed convection MHD flow of nanofluid containing different shapes of nanoparticles in a channel filled with saturated porous medium," *Nanoscale Research Letters*, vol. 10, no. 1, pp. 1–14, 2015.

[9] A. Hussanan, M. Z. Salleh, I. Khan, and S. Shafie, "Convection heat transfer in micropolar nanofluids with oxide nanoparticles in water, kerosene and engine oil," *Journal of Molecular Liquids*, vol. 229, pp. 482–488, 2017.

[10] A. Khalid, I. Khan, and S. Shafie, "Exact solutions for free convection flow of nanofluids with ramped wall temperature," *The European Physical Journal Plus*, vol. 130, no. 4, pp. 1–14, 2015.

[11] F. Ali, M. Gohar, and I. Khan, "MHD flow of water-based Brinkman type nanofluid over a vertical plate embedded in a porous medium with variable surface velocity, temperature and concentration," *Journal of Molecular Liquids*, vol. 223, pp. 412–419, 2016.

[12] N. A. M. Zin, I. Khan, and S. Shafie, "The impact silver nanoparticles on MHD free convection flow of Jeffrey fluid over an oscillating vertical plate embedded in a porous medium," *Journal of Molecular Liquids*, vol. 222, pp. 138–150, 2016.

[13] A. R. Bestman, "Natural convection boundary layer with suction and mass transfer in a porous medium," *International Journal of Energy Research*, vol. 14, pp. 389–396, 1990.

[14] X. Guo, J. Cai, and X. Yu, "Kinetics and thermodynamics of microalgae residue oxidative pyrolysis based on double distributed activation energy model with simulated annealing method," *Journal of Analytical and Applied Pyrolysis*, vol. 154, 2021.

[15] T. Hayat, A. Aziz, and A. Alsaedi, "Analysis of entropy production and activation energy in hydromagnetic rotating flow of nanoliquid with velocity slip and convective conditions," *Journal of Thermal Analysis and Calorimetry*, vol. 146, no. 6, pp. 2561–2576, 2021.

[16] N. R. Araújo, Á. C. Duarte, F. J. Pujatti, M. B. Freitas-Marques, and R. C. Sebastião, "Kinetic models and distribution of activation energy in complex systems using Hopfield neural network," *Thermochimica Acta*, vol. 697, article 178847, 2021.

[17] E. Elangovan and S. K. Natarajan, "Effects of pretreatments on quality attributes, moisture diffusivity, and activation energy of solar dried ivy gourd," *Journal of Food Process Engineering*, vol. 44, no. 4, 2021.

[18] M. Bilal, A. Saeed, M. M. Selim, T. Gul, I. Ali, and P. Kumam, "Comparative numerical analysis of Maxwell's time-dependent thermo-diffusive flow through a stretching

cylinder," *Case Studies in Thermal Engineering*, vol. 27, article 101301, 2021.

[19] A. Saeed, A. Alsubie, P. Kumam, S. Nasir, T. Gul, and W. Kumam, "Blood based hybrid nanofluid flow together with electromagnetic field and couple stresses," *Scientific Reports*, vol. 11, no. 1, pp. 1–18, 2021.

[20] J. R. Platt, "Bioconvection patterns in cultures of free-swimming organisms," *Science*, vol. 133, no. 3466, pp. 1766-1767, 1961.

[21] A. V. Kuznetsov, "Thermo-bioconvection in a suspension of oxytactic bacteria," *International Communications in Heat and Mass Transfer*, vol. 32, no. 8, pp. 991–999, 2005.

[22] I. Tlili, M. Ramzan, H. U. Nisa, M. Shutaywi, Z. Shah, and P. Kumam, "Onset of gyrotactic microorganisms in MHD micropolar nanofluid flow with partial slip and double stratification," *Journal of King Saud University-Science*, vol. 32, no. 6, pp. 2741–2751, 2020.

[23] F. S. Al-Mubaddel, U. Farooq, K. Al-Khaled et al., "Double stratified analysis for bioconvection radiative flow of Sisko nanofluid with generalized heat/mass fluxes," *Physica Scripta*, vol. 96, no. 5, article 055004, 2021.

[24] A. Abbasi, F. Mabood, W. Farooq, and M. Batool, "Bioconvective flow of viscoelastic nanofluid over a convective rotating stretching disk," *International Communications in Heat and Mass Transfer*, vol. 119, 2020.

[25] S. A. Shehzad, M. G. Reddy, A. Rauf, and Z. Abbas, "Bioconvection of Maxwell nanofluid under the influence of double diffusive Cattaneo–Christov theories over isolated rotating disk," *Physica Scripta*, vol. 95, no. 4, article 045207, 2020.

[26] S. Aziz, I. Ahmad, S. U. Khan, and N. Ali, "A three-dimensional bioconvection Williamson nanofluid flow over bidirectional accelerated surface with activation energy and heat generation," *International Journal of Modern Physics B*, vol. 35, no. 9, article 2150132, 2021.

[27] M. Alizadeh and D. D. Ganji, "Multi-objective optimization of an externally finned two-phase closed thermosyphon using response surface methodology," *Applied Thermal Engineering*, vol. 171, article 115008, 2020.

[28] M. Alizadeh and D. D. Ganji, "Heat transfer characteristics and optimization of the efficiency and thermal resistance of a finned thermosyphon," *Applied Thermal Engineering*, vol. 183, article 116136, 2021.

[29] S. Xun, J. Zhao, L. Zheng, X. Chen, and X. Zhang, "Flow and heat transfer of Ostwald-de Waele fluid over a variable thickness rotating disk with index decreasing," *International Journal of Heat and Mass Transfer*, vol. 103, pp. 1214–1224, 2016.

[30] H. I. Andersson, E. D. Korte, and R. Meland, "Flow of a power-law fluid over a rotating disk revisited," *Fluid Dynamics Research*, vol. 28, no. 2, pp. 75–88, 2001.

[31] C. Y. Ming, L. C. Zheng, and X. X. Zhang, "Steady flow and heat transfer of the power-law fluid over a rotating disk," *Communications in Heat and Mass Transfer*, vol. 38, no. 3, pp. 280–284, 2011.

[32] S. Z. Abbas, M. I. Khan, S. Kadry, W. A. Khan, M. Israr-Ur-Rehman, and M. Waqas, "Fully developed entropy optimized second order velocity slip MHD nanofluid flow with activation energy," *Computer Methods and Programs in Biomedicine*, vol. 190, article 105362, 2020.

[33] M. I. Khan, F. Alzahrani, A. Hobiny, and Z. Ali, "Fully developed second order velocity slip Darcy-Forchheimer flow by a variable thicked surface of disk with entropy generation," *International Communications in Heat and Mass Transfer*, vol. 117, article 104778, 2020.